JOURNAL OF PROPULSION AND POWER
Vol. 23, No. 4, July–August 2007

Manufacturing and Performance of Nanometric Al/MoO_3 Energetic Materials

Kevin C. Walter*
Scientific Applications & Research Associates, Inc., Cypress, California 90630
David R. Pesiri†
Los Alamos National Laboratory, Los Alamos, New Mexico 87545
and
Dennis E. Wilson‡
Energetic Materials and Products, Inc., Austin, Texas 78758

DOI: 10.2514/1.25461

Nanometric powders of aluminum (Al) and molybdenum trioxide (MoO_3) have been combined to create an inorganic energetic material. When optimized, the burn rate of these materials (~400 m/s) exceeds that of conventional thermites (based on micron-sized powders), but is less than that of conventional explosives. Similar burn rates around 350 m/s are measured for these "superthermites" using n–Al powder in the size range between 30 and 90 nm in diameter (20–60 m^2/g, 60–80 wt % Al) and an oxygen-to-fuel mass ratio of 1.4. The burn rate decreases when the surface area of the MoO_3 is decreased from 64 to 40 m^2/g, or when oxygen to fuel is changed from 1.2. Thus, for each average particle diameter, there is an optimum burn rate at an oxygen-to-fuel ratio that depends on the wt % Al present in the material and the particle size distribution of the powder. The burn rate is dependent on several materials and processing factors such as the quality of the nanometric ingredients, the processing method, and exposure to air and light, so the effect of aging and environmental exposure on the individual ingredients has been investigated. The results of this powder aging study suggests that the surface area of n–MoO_3 can decrease twofold within 10–12 days, and the Al-metal content in n–Al can decrease as much as 50% over two years. Adequate handling and storage procedures must therefore be followed for the effective use of nanometric powders and their superthermite mixes.

Introduction

THE study of superthermites made from nanometric powders began at Los Alamos National Laboratory in the mid-1990s, resulting in the first patent in the field [1], and ongoing work at numerous federal and private institutions has taken place [2–6]. Most applications take advantage of superthermite's high burn rate, high heat production, negligible gas generation, and nontoxic properties [7–11]. Various routes of manufacturing, storing and testing of superthermites have been reported, with each aspect potentially affecting the performance, and thus their potential commercial success.

Technically, superthermites or nanothermites belong to a class of energetic materials called pyrotechnics, as do their micron-scale cousins. Pyrotechnics operate by combustion processes, in which a fuel combines with oxygen to release heat, light, smoke, or gas. If the reactants are pure and if the mixture is homogeneous on a scale comparable to the length scale of the individual reactants, then according to Cooper and Kurowski [12], the burning rate (i.e., the combustion wave speed), for a given pyrotechnic is a function of 1) porosity, 2) particle size, and 3) stoichiometry. In addition, 4) confinement of a pyrotechnic mixture can also affect its behavior by "speeding up" the combustion process by concentrating heat and hot gas in the reaction zone.

Historically, thermites are considered to be a subset of pyrotechnics. The term thermite originally referred to an aluminum and iron oxide reaction. Today a thermite reaction implies any exothermic reaction, which involves a metal reacting with a metal oxide to form a more stable oxide. The fuels are metals, generally aluminum, and the oxidizers are metal oxides or salts. For conventional thermites, the reaction rates, for example, the combustion wave speeds are much less than the bulk sound speed in the unreacted material and they generally produce very little gas. Conventional thermite reactions are difficult to ignite and proceed so slowly that most of the released energy is dissipated so that the primary effect is an increase in temperature with very little gas production. The primary distinguishing features of superthermite reactions are 1) their high rate of energy release, 2) they can produce considerable blast due to their intermediate gas phase of the reaction products, and 3) their ignition sensitivity. In addition, their output is a strong function of particle size and it is these nanoscale characteristics that create a unique energetic classification for superthermites.

From 2000 to 2003, two companies, Technanogy, LLC and Technanogy Materials Development, LLC, manufactured n–Al, an important component of superthermite, and the superthermite itself. This paper is a review of their efforts to reproducibly manufacture and test superthermites, and their understanding of the environmental effects (aging) of the superthermite ingredients. The paper also compares the results to the performance predicted by the most popular theory describing the burn rate of nanometric thermites.

Experimental Details

Superthermites were manufactured from various lots of n–Al and n–MoO_3. The n–Al was manufactured by Technanogy Materials Development using a gas condensation method described elsewhere [4]. The MoO_3 was obtained from Climax Molybdenum Marketing Corporation in Tempe, Arizona. Details of the superthermite ingredients and designations are listed in Table 1. The specific surface area σ of n–Al was measured by nitrogen gas adsorption using a Micromeritics Tristar 3000 gas analyzer and after degassing

Received 26 May 2006; revision received 5 February 2007; accepted for publication 30 March 2007.

*Director, Chemical and Directed Energy Programs.
†Technology Transfer Executive, Technology Transfer Office.
‡CEO and Founder.

Table 1 Characteristics of the superthermite ingredients, designations, and mixing parameters for each trial mix (TM) used in this study

		n–Al				
Trial	n–MoO_3 m^2/g	σ, m^2/g	Diameter, nm	Oxide thickness, nm	wt % Al	O/F ratio
TM-06	64	46.9	44.7	2.7	63.9	1.2
TM-07	40	46.9	44.7	2.7	63.9	1.2
TM-10	64	12.1	168.1	5.9	73.5	1.2
TM-13	64	12.1	168.1	5.9	73.5	1.4
TM-14	64	22.1	93.1	2.8	76.8	1.4
TM-16	64	23.7	91.0	2.7	81.0	1.4
TM-18	64	46.9	44.7	2.7	63.9	1.4
TM-19	40	46.9	44.7	2.7	63.9	1.4
TM-20	64	46.9	44.7	2.7	63.9	1.2
TM-21	40	46.9	44.7	2.7	63.9	1.2
TM-23	64	59.9	32.3	1.9	59.5	1.4
TM-25	64	15.7	138.7	2.7	87.2	1.4
TM-26	64	31.4	65.3	2.1	75.7	1.4
TM-27	64	31.4	65.3	2.1	75.7	1.2
TM-28	64	46.9	44.7	2.7	63.9	1.2
TM-29	64	59.9	32.3	1.9	59.5	1.2

under nitrogen at an elevated temperature (10°C/ min ramp to 100°C and hold for 1 h followed by 10°C/ min ramp to 200°C and hold for 2 h). The specific surface area of n-MoO_3 was similarly measured after a slightly different degas procedure (10°C/ min ramp to 100°C and hold for 3 h). The surface area was determined using the Brunauer, Emmett, and Teller (BET) method and had an accuracy of ±2.5%. The weight gain Δm of the n–Al powder upon oxidation was measured by thermogravimetric analysis of the powders using a Perkin-Elmer Pyris I TGA (thermogravimetric analyzer). Approximately 3.0 mg of powder was heated at 10°C/ min to 30°C and held for 2 min, heated at 10°C/ min to 900°C, and held at 900°C for 6 h. The oxidizing gas was 25% oxygen in argon flowing at 30 sccm. Similar results can be obtained using oxygen/argon mixtures with as little as 8% oxygen, so the gas composition is not believed to be important if the oxygen concentration is between 8 and 25%, and no nitrogen is present. The TGA analysis has an accuracy of ±5%. Assuming spherical particles all the same size, the weight percent aluminum, average particle diameter, and oxide thickness are calculated using Eqs. (1–4),

$$\text{wt \%Al} = \frac{2A_{\text{Al}}\Delta m}{3A_{\text{O}}} \tag{1}$$

$$\beta = \frac{V_{\text{ox}}}{V_{\text{Al}}} = \frac{\rho_{\text{Al}}}{\rho_{\text{ox}}}\left(\frac{3A_{\text{O}}}{2A_{\text{Al}}}\frac{100}{\Delta m} - 1\right) \tag{2}$$

$$d = \frac{6(1+\beta)}{\sigma(\rho_{\text{Al}} + \beta\rho_{\text{ox}})} \tag{3}$$

$$t = \frac{3(1+\beta)^{2/3}}{\sigma(\rho_{\text{Al}} + \beta\rho_{\text{ox}})}[(1+\beta)^{1/3} - 1] \tag{4}$$

where the atomic weight of aluminum A_{Al} is 27 g/mol; the atomic weight of oxygen A_{O} is 16 g/mol; the density of aluminum ρ_{Al} is 2.7 g/cm^3; and the density of the aluminum oxide layer ρ_{ox} is 3.2 g/cm^3 (calculated from pycnometry measurements). This combination of equations allows a unique combination of particle diameter d and oxide thickness t to be calculated from TGA and BET measurements that correct for the effects of differing oxide layer thickness on particles of similar diameter.

The oxide to fuel ratio (O/F ratio) is the mass ratio of the n–MoO_3 and n–Al powders used in each trial mixture (TM). A number of mixes were prepared at different O/F values to identify the optimum burn-rate performance. The optimum ratio for pure materials would be 2.667. However, the optimum ratio for the materials tested is understandably decreased by multiplying by the fraction of aluminum metal in the powder. A further reduction of approximately 30% in the O/F value is empirically shown to optimize superthermite burn rates (see later results).

Production of the superthermite is a hazardous process that should only be performed by skilled personnel using proper equipment and adequate safety measures. Batches of approximately 1 g were made in the following manner. First, n–Al and n–MoO_3 powders were weighed out into a 250 mL stainless steel beaker. The powder was then wetted with approximately 65–70 g of hexane. An initial dispersion of the n–Al/n–MoO_3 mixture was accomplished by hand stirring the mixture with a stainless steel spatula, followed by 2 min in a 70 W ultrasonic bath (Bransonic Ultrasonic Cleaner model 1510R-DTH). The beaker was removed from the bath and the mixture further dispersed using an ultrasonic horn (Branson Sonifier 450 W supply with a 1/2 in. probe tip) for 15 min at power setting 8 and 50% duty cycle. The temperature of the solution, as measured by a thermocouple probe, increased to 50–55°C during sonication. Approximately 100 g of hexane was added during sonication to reduce the viscosity of the mixture. Following sonication, the superthermite was allowed to settle out of the hexane. The excess hexane was decanted from the precipitated solids which were then placed in a modified Buchner funnel that contained a porous metal filter and vacuum filtered to near dryness for approximately 5 min. The mixed solids were then placed in a 60–80°C air oven for about 15 min to remove the remaining hexanes. The dry superthermite cake was then forced through a no. 50 metal sieve using gentle strokes with a blunted, thin metal blade. Superthermite powder was either immediately tested or stored in metal tins under dry argon until tested.

The burn rate of each TM was measured using a custom device. The superthermite powder (50–75 mg) was loaded into a narrow trough (5.7 l × 0.2 w × 0.2 h cm, volume = 0.22 cm^3) in a metal plate with 0.1 mm diam holes spaced 1.4 cm apart along the length of the trough. A second plate, with 0.1 mm diam holes spaced 1.4 cm (0.5 in.) apart, was positioned below the trough, with a glass slide in between, so that the holes ran along the length of the sample. Photodiodes were placed below each of the four holes, and connected to an oscilloscope for data collection. A low-power source and switch were used to generate an electrical spark sufficient to ignite the superthermite on one end of the trough. As the superthermite burned along the trough, the photodiodes registered the passage of the light generated and allowed a measurement of the time between signals at sequential diodes. A burn rate for each TM was determined by calculating a rate between three pairs of holes and averaging the results.

Results and Discussion

The burn-rate results, along with relevant ingredient details, are listed in Table 2 and graphed in Fig. 1. In Fig. 1, burn-rate data are

Table 2 TM burn rates, powder, and O/F details

TM	n–MoO_3, m^2/g	n–Al diameter, nm	O/F ratio	Burn rate, m/s
TM-06	64	44.7	1.2	414.9
TM-07	40	44.7	1.2	361.1
TM-10	64	168.1	1.2	161.8
TM-13	64	168.1	1.4	158.6
TM-14	64	93.1	1.4	340.8
TM-16-1	64	91.0	1.4	338.8
TM-16-2	64	91.0	1.4	354.5
TM-18	64	44.7	1.4	328.4
TM-19	40	44.7	1.4	343.7
TM-20	64	44.7	1.2	396.6
TM-21	40	44.7	1.2	363.8
TM-23-1	64	32.3	1.4	359.0
TM-23-2	64	32.3	1.4	312.1
TM-25	64	138.7	1.4	262.6
TM-26	64	65.3	1.4	420.0
TM-27	64	65.3	1.2	326.5
TM-28	64	44.7	1.2	442.5
TM-29	64	32.3	1.2	393.4

plotted as a function of the mean n–Al particle diameter as calculated using Eq. (3) and the data in Table 1. Variation in burn rate due to changes in the O/F ratio can be seen by evaluating the vertical collections of data points for each particle diameter. Beginning with 44.7 nm diameter data, it is clear that an O/F ratio of 1.2 (●) produces the highest burn rate.

Most of the data in Fig. 1 were taken using an O/F of 1.4 (□). Note that the burn rate was approximately constant (300–350 m/s) across all n–Al diameters until the particle diameter exceeds 100 nm, and then decreases to about 150 m/s when $d = 168.1$ nm (O/F = 1.4). The reason for this decrease is unclear, although the effect of particle size distribution has been suggested.

The reproducibility of the burn-rate data is also illustrated in Fig. 1. The data corresponding to a particle diameter of 91.0 nm contain two data points at the highest burn rate (□) that show a very slight variation when two burn-rate tests are done on the "same" superthermite mix (TM-16-1 and -2). The result is very similar to that for a slightly higher n–Al diameter at $d = 93.1$ nm (TM-14). Referring to the data at $d = 44.7$ nm, the top three data points (●) were taken using three different superthermite batches (TM-06, TM-20, and TM-28) using the same n–Al and n–MoO_3. These three points suggest a batch-to-batch variation of about 12%, although there are not sufficient data points to be statistically significant. Finally, the bottom two data points (□) in the $d = 32.3$ nm data set are from two batches made with identical powders, but with the lowest point being sonicated at a 7.5 power setting, rather than at 8.

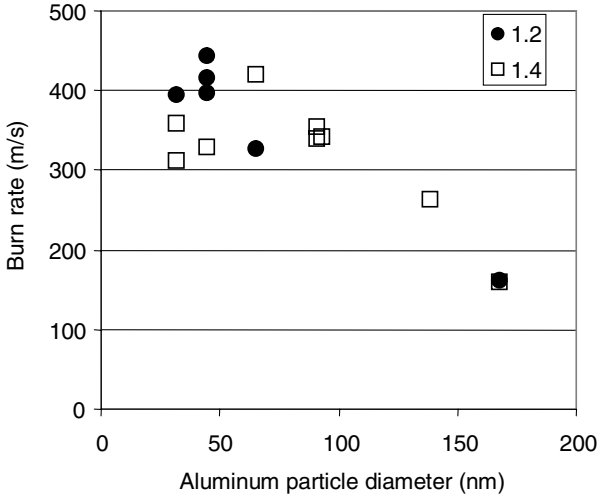

Fig. 1 Plot showing burn-rate dependency on n–Al diameter and O/F ratio using n–MoO_3 (64 m^2/g). ● indicates an O/F ratio of 1.2, and □ indicates on O/F ratio of 1.4.

Superthermite Combustion Behavior

The combustion wave speed of superthermites is a function of a number of different variables, which can be grouped into the following three basic categories: *morphology*, which refers to the microstructure, or geometry of the reaction pairs; *confinement*, which refers to the degree of geometrical confinement of the container; and *thermochemistry*. These groups and subgroups are as follows:

1) Morphology
   a) mean particle size;
   b) particle shape, for example, flakes or sheets vs spheres;
   c) porosity or degree of consolidation;
   d) oxide layer thickness, which affects available aluminum content.
2) Confinement
3) Thermochemistry
   a) stoichiometry or equivalence ratio;
   b) particular reaction pairs, which affect adiabatic temperature, heat of combustion, and the equilibrium thermodynamic state of products.

In defining these variables, we are assuming that the mixture is pure and homogeneous. In addition, we will assume a standard lognormal distribution so that the mean particle size as defined by analytical methods such as BET completely characterize the nanoparticles.

A useful way of classifying superthermite combustion behavior is to first form four groups based upon two key characteristics, namely, confinement and *degree of consolidation*, which are defined below.

Degree of Consolidation (Porosity)

Unconsolidated refers to superthermites, which have not been pressed. The density of these "loose" powders varies from approximately 5–10% of the bulk or the theoretical maximum density (TMD). The lower value corresponds to powder that has been poured into a container, and the upper value corresponds to powder which has been subjected to vibration but not subjected to a mechanical pressure.

Consolidated powder refers to superthermites, which have been compressed by placing it into a mold and subjecting to a mechanical pressure such that its density is 30–80% of TMD. We arbitrarily define the lower limit; however, the theoretical packing density of spheres fixes the upper limit.

Confinement

Unconfined superthermites are defined as mixtures that are exposed to ambient conditions, usually air at or near STP.

Confined superthermites are defined as mixtures contained within an enclosure that maintains its structural integrity during ignition and burning, for example, a tube with one open end where the ignition occurs at the closed end, for example, a shock tube type geometry.

Wilson and Kim have published three different theoretical models [13–15] for the combustion wave speed for confined–unconsolidated, confined–consolidated, and unconfined–consolidated categories. These models have one feature in common, namely, they are all one dimensional, which greatly simplifies the analysis.

A detailed model for the present case of an unconfined and unconsolidated mixture is more complex due primarily to the multidimensional nature of the process and the difficulty in writing accurate boundary conditions on the free surface. There are no known mathematical models for this case; however, we can obtain a useful nondimensional result, if we model the combustion process as quasi one dimensional. Referring to Fig. 2, a simple energy balance across the phase change zone results in the following equation:

$$\phi\bar{h}(T_{gc} - T_{sm}) + \varepsilon\sigma_{sb}\left(T_{gc}^4 - T_{sm}^4\right) + (1-\phi)\frac{k_s}{d_{eff}}\frac{dT_s}{dz}\bigg|_{z=0} = \rho_s U_C h_L \tag{5}$$

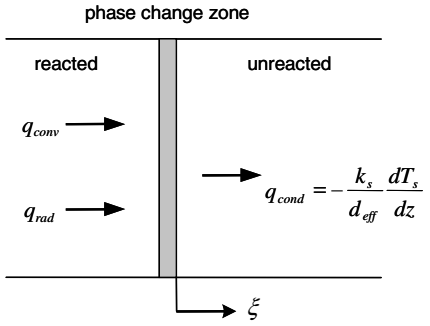

Fig. 2 The observed burn-rate behavior is predicted by an equation that is inversely proportional to the mean or effective particle diameter of the superthermite mixture.

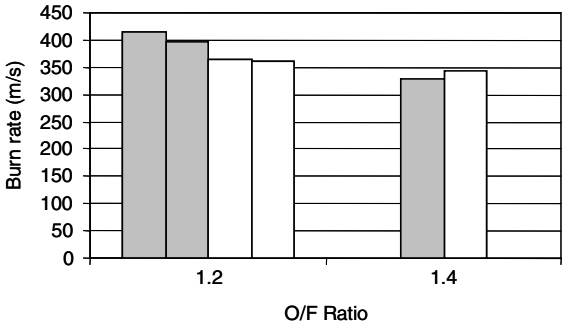

Fig. 3 Plot of burn rate versus O/F for superthermites using 44.7 nm n–Al and 64 m^2/g (gray) and 40 m^2/g (white) grades of n–MoO_3.

where

$$h_L = h_{\text{fs}}|_{\text{Al}} + h_{\text{sg}}|_{\text{MoO}_3} \tag{6}$$

ϕ is the porosity, σ_{sb} is the Stefan–Boltzman constant, ρ_s is the density of the solid, ε is the emissivity, d_{eff} is the average particle diameter, k_s is the thermal conductivity of solid aluminum, h is the enthalpy, $\bar{h}$ is the convective heat transfer coefficient, T is the temperature, and U_C is the combustion wave speed. In Eq. (5), the subscripts "gc" and "sm" are for the gas phase combustion temperature and solid phase melting temperature, respectively. In Eq. (6), the subscripts "fs" and "sg" refer to the phase change enthalpy from the solid to liquid state and solid to gas state, respectively. The convective heat transfer coefficient can be estimated from the following empirical correlation of the Nusselt number Nu by

$$Nu_{d_{\text{eff}}} = \frac{\bar{h}d_{\text{eff}}}{k_s} = 2 + 1.1Re_{d_{\text{eff}}}^{0.6}Pr^{1/3} \tag{7}$$

where Pr is the Prandtl number and Re is the Reynolds number.

This energy balance equation can be used to determine an expression for the combustion wave speed. As such, it deserves some discussion. In deriving this equation we have assumed that the molybdenum trioxide sublimates in the phase change zone and account for this by its enthalpy of sublimation. For the aluminum, however, we account only for the enthalpy associated with melting. This assumption is somewhat arbitrary; however it is consistent with differential scanning calorimeter experiments on aluminum nanoparticles, which show ignition and burning at temperatures of 450°C, which is well below melting for bulk aluminum. If the effective particle diameter is sufficiently small, we can neglect the Reynolds number dependence. Therefore, the boundary condition at the combustion front becomes

$$\phi\frac{2k_g}{d_{\text{eff}}}(T_{\text{gc}} - T_{\text{sm}}) + \varepsilon\sigma_{\text{sb}}\left(T_{\text{gc}}^4 - T_{\text{sm}}^4\right) + (1-\phi)\frac{k_s}{d_{\text{eff}}}\frac{dT_s}{dz}\bigg|_{z=0} = \rho_s U_c h_L \tag{8}$$

where k_g is the thermal conductivity of the gas.

This simple equation can now be used to help interpret the observed burn rates. If the radiation term is neglected, then the following equation for the nondimensional combustion wave speed results:

$$\frac{U_C d_{\text{eff}}}{\alpha_s} = \text{function}(\phi, k_g/k_s) \tag{9}$$

Equation (9) predicts a burn rate that is inversely proportional to the mean or effective particle diameter of the superthermite mixture, which approximates the observed behavior shown in Fig. 2. In writing this simple equation, we assumed spherical particles and have neglected many of the other effects, such as stoichiometry and oxide layer thickness.

Aging Characteristics

Figure 3 shows the effect of changing the surface area of the n–MoO_3 and O/F ratio. Note that decreasing the n–MoO_3 surface area causes a reduction in burn rate for optimized superthermites with an O/F of approximately 1.2. However, the surface area effect can be compensated for, and perhaps even reversed, by increasing O/F to near 1.4 if a decrease in the burn rate is acceptable. Although the two n–MoO_3 powders are from different shipments from Climax Moly, and were routinely stored in dry argon and shielded from light, measurements indicated that the n–MoO_3 ages with exposure to light and air. Aging is evidenced by a decrease in measured surface area.

Storage of MoO_3 powder in a nonairtight container, with occasional exposure to air during material removal for experiments, reduced the surface area by more than 2 times within the first 200 days. After 200 days, the rate of degradation is slower. Surface area reduction can be quite rapid, especially for higher surface area powders. The surface area of MoO_3, initially at 70 m^2/g, fell below 40 m^2/g after only 12 days in a nonairtight container and exposed to light. However, the surface area of MoO_3 powder was invariant for more than 500 days (the longest duration that was tested), if the powder was kept in an airtight metal can (no light exposure) and under argon.

The characteristics of n–Al powder can also change over time, although not as much as for n–MoO_3. Table 3 shows how the characteristics of four powders changed with time when stored in clear glass vials with nonairtight lids. Generally, the particle diameter

Table 3 Lot numbers, elapsed time, and changing characteristics of some n–Al powders. Errors in Δm (measured by TGA) and σ (via BET) are ±5% and ±2.5% respectively. Errors in all other values [using Eqs. (1–4)] are from error propagation calculations

Powder	Time, day	Δm, %	σ, m^2/g	$\beta = V_{\text{ox}}/V_{\text{Al}}$	d, nm	t, nm	wt % Al
B030301	0	47.9	61.3	0.58 ± 0.06	30.9 ± 3.4	2.2 ± 0.4	53.9 ± 2.7
	931	46.8	62.0	0.76 ± 0.08	33.2 ± 4.0	2.8 ± 0.5	52.7 ± 2.6
B032401	0	11.9	75.4	4.40 ± 0.25	21.3 ± 2.6	4.6 ± 0.5	13.4 ± 0.7
	910	11.7	76.4	5.57 ± 0.32	25.1 ± 3.1	5.9 ± 0.6	13.2 ± 0.7
B040201	0	23.7	47.2	1.87 ± 0.13	36.0 ± 4.2	5.3 ± 0.6	26.7 ± 1.3
	901	17.5	43.7	0.34 ± 0.02	44.5 ± 2.6	8.7 ± 0.9	19.7 ± 1.0
B040301	0	72.4	23.6	0.15 ± 0.04	88.6 ± 9.1	2.1 ± 0.7	81.5 ± 4.1
	900	31.6	24.2	1.53 ± 0.12	82.6 ± 10.2	11.0 ± 1.5	35.6 ± 1.8

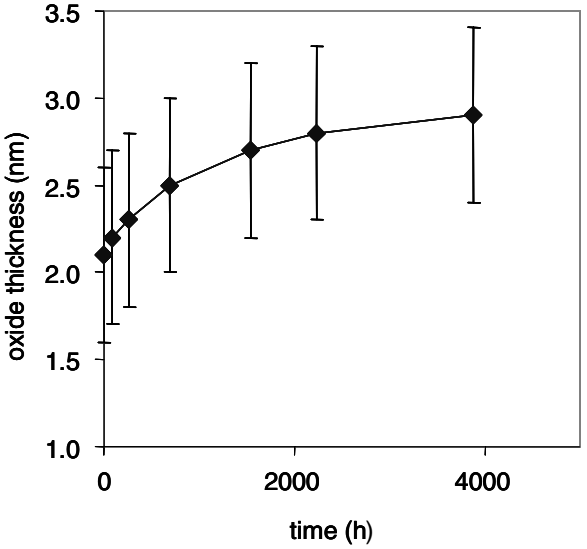

Fig. 4 Plot of oxide coating thickness versus time for n–Al powder during storage in a nonairtight clear glass vial. Note the error bar is ±0.5 nm.

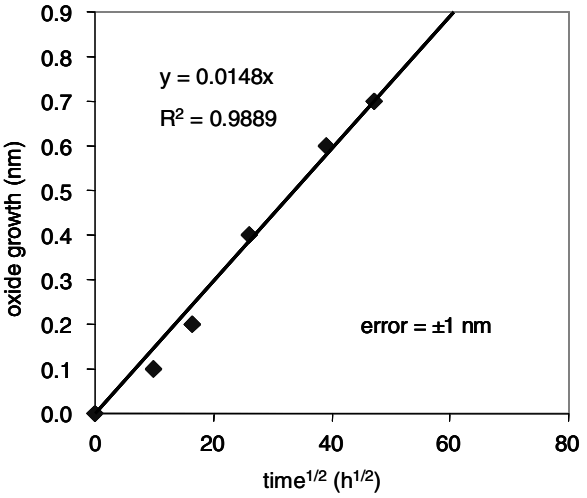

Fig. 5 Plot of the oxide growth versus time$^{1/2}$ showing the linear relationship supporting a conventional diffusion mechanism for thickening of the oxide layer.

and oxide thickness increase, and the wt % Al decreases over time in a predictable manner. Assuming a spherical particle of Al ($\rho = 2.7$ g/cm^3) that completely reacts to form Al_2O_3 ($\rho = 3.2$ g/cm^3), the particle diameter will increase by a maximum of 17%. The values in Table 3 indicate that uncertainties in the measurements, and especially the surface area measurement, limit the accuracy of the particle diameter determination and limit the ability to detect small changes in diameter.

The uncertainty in the diameter is mostly due to uncertainty in the surface area measurement. The assumptions in the BET model for gas adsorption onto a surface, and assumptions of particles with smooth surfaces (no cracks or defects), require further study to determine if the specific area surface measurement can be improved. Secondly, it is unknown if the thickening of the oxide layer also changes the particle's surface roughness, and thus the measurable surface area. Special note should be made that the 5% error in the TGA measurement still allows calculation of the oxide thickness to within a nanometer or less. This accuracy is notable because it is better than that possible with most transmission electron microscopy techniques.

Figure 4 shows a plot of the oxide thickness calculated for n–Al powder (39 nm, 1.8 nm oxide initially) during storage in a nonairtight clear glass vial. The calculation assumes no change in specific surface area during aging. Note that even after about 4000 h, the oxide thickness barely increases more than the error in the measurement (±0.5 nm). Even so, most of the oxide thickening occurs within 2000 h (less than 90 days). Figure 5 plots the change in oxide thickness against time$^{1/2}$. The linear relationship clearly demonstrates the expected time dependence for Fickian diffusion.

IV. Conclusions

The burn-rate data show that there is no observable difference in the performance of a superthermite made with 30 or 90 nm n–Al powder, and the optimum ratio for mixing the oxidizer (O) and n–Al fuel (F) is O/F = 1.2. Thus, applications requiring high superthermite burn rates should be able to use any n–Al powder with a mean diameter between 30 and 90 nm. The results show that for each n–Al particle diameter there is an optimum burn rate at an O/F ratio that depends on the wt % Al present in the material and presumably, the particle size distribution of the powder. The surface area of the n–MoO_3 should be as high as possible, but determination of the optimum surface area has not been accomplished. Both nanopowders clearly change with exposure to air and/or light, so it is reasonable to assume that a superthermite's performance will also change with exposure to air and/or light. The surface area of n–MoO_3 decreases by 2× within 12 days, and the Al-metal content in the n–Al decreases up to 50% after 2 years. This study, however, does not include any aging data on superthermite mixtures. Other metal oxides with high surface area exist and should be studied for resistance to aging effects.

The manufacture of superthermites is complicated and a multistep process that requires extreme attention to all processing details if reproducible performance is to be achieved. It is likely that widely varying burn-rate results can be avoided by improvements in the processing protocols, and these changes could have an even greater effect on burn rate than particle diameter or surface area. The use of ingredients whose properties change with time and exposure to the atmosphere obviously complicate the manufacturing issues. Even so, conventional pyrotechnic ingredients have similar handling and exposure issues, so environmental sensitivity alone should not deter further development.

The error associated with surface area and thermogravimetric analysis of n–Al is reported. Although improvements in surface area measurement could provide the most significant improvement in accuracy, the wt % Al and oxide thickness t are currently being measured with an accuracy similar to that available only through more exotic techniques (e.g., transmission electron microscopy). The oxide coating thickness has been shown to increase with time with exposure to air, however. Thickening of the oxide coating can be reduced by routinely packaging and storing n–Al in airtight metal cans under oxygen-free gas. Although these efforts certainly reduce the aging rate, measurements indicate these efforts are not sufficient to completely eliminate aging, and oxide thickness can also increase during storage. Thus, reanalyzing n–Al powder after about 1 year in storage is recommended.

Acknowledgements

The authors wish to recognize the extensive contributions of Chris Aumann, Doug Carpenter, and Ed O'Neill, all former employees of Technanogy Materials Development. The authors are grateful to the guest editor, Steve Son, for inviting our contribution.

References

[1] U.S. Patent 5,717,159, filed 19 Feb. 1997.

[2] Son, S. F., Hiskey, M. A., Naud, D. L., Busse, J. R., and Asay, B. W., *Proceedings of the International Pyrotechnics Society, The Twenty-Ninth International Pyrotechnics Seminar*, 14–19 July 2002, pp. 871–877.

[3] Bockman, B., Son, S. F., Asay, B. W., Busse, J. R., Peterson, P. D., Mang, J. T., and Pantoya, M., *38th Combustion Subcommittee Proceedings*, JANNAF, Destin, FL, 4–8 April 2002.

[4] Pesiri, D., Aumann, C. E., Bilger, L., Booth, D., Carpenter, R. D., Dye, R., O'Neill, E., Shelton, D., and Walter, K. C., "Industrial Scale Nano-Aluminum Powder Manufacturing," *Journal of Pyrotechnics* (submitted for publication).

[5] Bockman, B. S., Pantoya, M. L., Son, S. F., Asay, B. W., and Mang, J. T., "Burn Rates and Propagation Mechanisms of Metastable Intermolecular Composites," *Combustion and Flame* (submitted for publication).

[6] Higa, K. T., Bliss, D. E., and Johnson, C. E., "Aging of Nanoscale Aluminum Powders and Composites," *Propellants, Explosives and Pyrotechnics* (submitted for publication).

[7] Granier, J. J., and Pantoya, M. L., "Laser Ignition of Nanocomposite Thermites," *Combustion and Flame*, Vol. 138, 2004, pp. 373–383.

[8] Pantoya, M. L., and Granier, J. J., "Combustion Behavior of Highly Energetic Thermites: Nano Versus Micron Composites," *Propellants, Explosives, Pyrotechnics*, Vol. 20, 2005, pp. 53–61.

[9] Schoenitz, M., Ward, T. S., and Dreizin, E. L., "Fully Dense Nano-Composite Energetic Powders Prepared by Arrested Reactive Milling," *Proceedings of the Combustion Institute*, Vol. 30, 2005, pp. 2071–2078.

[10] Tillotson, T. M., Gash, A. E., Simpson, R. L., Hrubesh, L. W., Satcher, J. H., Jr., and Poco, J. F., "Nanostructured Energetic Materials Using Sol-Gel Methodologies," *Journal of Nanocrystaline Solids*, Vol. 285, 2001, pp. 338–345.

[11] Valliappan, S., Swiatkiewicz, J., and Puszynski, J. A., "Reactivity of Aluminum Nanopowders with Metal Oxides," *Powder Technology*, Vol. 156, 2005, pp. 164–169.

[12] Cooper, P. W., and Kuroski, S. R., *Introduction to the Technology of Explosives*, VCH Publishers Inc., Weinham, 1996.

[13] Wilson, D. E., and Kim, K., "A Simplified Model for the Combustion of Al/MoO_3 Nanocomposite Thermites," AIAA Paper 2003-4536, 2003.

[14] Wilson, D. E., and Kim, K., "Propagation of Combustion Waves in Consolidated MIC Pellets," *JANNAF 32nd PEDCS and 21st SEPS Joint Meeting*, JANNAF, Destin, FL, July 2004.

[15] Wilson, D. E., and Kim, K., "Combustion of Consolidated and Confined Metastable Intermolecular Composites," AIAA Paper 2005-0275, 2005.

S. Son
Associate Editor